Comparison of Remazol Brilliant Blue Reactive Adsorption on Pristine and Calcined ZnAl, MgAl, ZnMgAl Layered Double Hydroxides

Suleiman Mohammed Gidado · İme Akanyeti

Abstract Layered double hydroxides (LDHs) are promising adsorbents for the removal of various contaminants from water. However, a comprehensive understanding of how ternary LDHs differ from the divalent ones in terms of dye adsorption capacity and the underlying mechanisms still remain unknown. Remazol brilliant blue reactive (RBBR) adsorption on pristine and calcined (C) ZnAl, MgAl, and ZnMgAl LDHs were comprehensively investigated for the first time in this study. The characteristics of the pristine and calcined samples were established with X-ray diffractometer, Fourier transform infrared spectrophotometer, zeta potential analyzer, and Brunauer–Emmett–Teller method. A considerably larger adsorption capacity was obtained with pristine MgAl (220 mg/g) and ZnAl (191 mg/g) compared to that of ZnMgAl (164 mg/g) at all studied initial dye concentrations (10–250 mg/L) and solution pH (3–12). However, when the LDH samples were calcined, the largest RBBR mass adsorbed was achieved with ZnMgAl-C (263 mg/g) followed by MgAl-C (247 mg/g) and ZnAl-C (236 mg/g). In comparison to the pristine samples, the faster adsorption rate and higher adsorption capacity of the calcined samples were attributed to the large specific surface area and enhanced electrostatic interactions due to the higher positive charge obtained after calcination. ZnMgAl-C had the largest surface area and the charge, explaining its superior adsorption capacity over the divalent LDHs. Pseudo-first-order, pseudo-second-order, and Elovich models described the kinetics data well while Freundlich and Redlich–Peterson isotherms suitably fit to the equilibrium data for the pristine and calcined LDHs. Surface adsorption via electrostatic interactions was found to be the effective mechanism for RBBR adsorption on all pristine and calcined LDHs while intercalation was not.

S. M. Gidado · İ. Akanyeti
Environmental Research Centre, Cyprus International University, North Cyprus via Mersin 10, Haspolat, Nicosia, Turkey

S. M. Gidado
Environmental Science, Institute of Graduate Studies and Research, Cyprus International University, North Cyprus via Mersin 10, Haspolat, Nicosia, Turkey

İ. Akanyeti (✉)
Environmental Engineering, Engineering Faculty, Cyprus International University, North Cyprus via Mersin 10, Haspolat, Nicosia, Turkey
e-mail: iakanyeti@ciu.edu.tr

1 Introduction

The release of synthetic dyes into water bodies by the effluents of various industries, such as textile, paper, leather tanning, food processing, plastics, cosmetics,

rubber, printing, and dye manufacturing, causes severe environmental pollution (Yagub et al. 2014). The accumulated persistent dyes in aquatic environments prevent the penetration of light into the water, hence affecting the photochemical activities (Malik and Grohmann 2012). Moreover, they can show carcinogenic and mutagenic effects on aquatic and human lives (Praveen et al. 2009). RBBR is among the reactive dyes, widely used for wool, fiber, and silk dying in textile industry and exhibits characteristics of toxicity, poor degradation, and carcinogenicity (Banat et al. 1996; Rezaee et al. 2008). The non-biodegradable and chemically stable characteristics of RBBR and similar dyes make them difficult to be removed from wastewater using conventional treatment processes (Wong and Yu 1999; Bediako et al. 2019). More so, about 10 to 200 mg/L concentration of reactive dyes are found in wastewater outlets (Paneysar et al. 2019). As the legal dye discharge requirements are getting more restricted (Malik and Grohmann 2012), elucidating efficient treatment methods in order to eliminate the dyes from effluent waters is essential to reduce environmental impacts. Adsorption, chemical oxidation, photodegradation, and microbial decoloration/degradation are among the various treatment methods studied extensively for the removal of dyes (Forgacs et al. 2004). All methods have their advantages and disadvantages in terms of efficiency, cost, and sustainability. Adsorption is considered an economically and technically viable process with a good performance at removing the synthetic dyes from water at low operating costs (Geethakarthi and Phanikumar 2011; Darmograi et al. 2015).

Layered double hydroxides (LDH) have received attention recently as high-capacity adsorbents for organic and inorganic water pollutants because of their large interlayer spaces, high anion exchange capacity, water-resistant structure, and high thermal stability (Sajid and Basheer 2016; Zhou et al. 2018; Ifebajo et al. 2020). LDH is represented by the formula of $[M^{2+}_{1-x} \times M^{3+}_{x} \times (OH)_2] \times [(A^{n-}_{x/n}) \times mH_2O]$, where M^{2+} represents divalent cations: Cu^{2+}, Mg^{2+}, Zn^{2+}, Ca^{2+}, Co^{2+}, and Ni^{2+}, while M^{3+} are of trivalent cations: Fe^{3+}, Al^{3+}, and Cr^{3+} and A^{n-} represent the interlayer anion such as OH^-, CO_3^-, NO_3^-, Cl^-, and SO_4^{2-} (Kowalik et al. 2013). Synthesis of LDH is economical due to the common and abundant metals in their structure. Faster kinetics and full regeneration capacities in a short time for reuse are the advantages of LDH compared to other adsorbents (Goh et al. 2008).

The adsorption of both positively and negatively charged dyes on LDH made of different metal hydroxide combinations and prepared by various methods has been studied extensively (Zheng et al. 2012; De Sá et al. 2013; Guo et al. 2013; Shan et al. 2015; Abdellaoui et al. 2017; Berner et al. 2018; Sheng et al. 2019; Zhu et al. 2019, Liu et al. 2019). MgAl and ZnAl are among the most commonly studied LDHs due to the availability and relatively lower cost of the metals used (Theiss et al. 2016). Recently, ternary and quaternary prepared LDHs were argued to be better than the traditional LDHs because of the improved redox and acid-base properties after the isomorphic substitution of another metal (Zaghouane-Boudiaf et al. 2012; Wang et al. 2016). Zheng et al. (2012) argued that the interlayer charge density was increased when Zn was incorporated into MgAl to obtain ZnMgAl-LDH and the produced ternary LDH achieved 98% removal of methyl orange. Similarly, in the study of Dudek et al. (2012), the adsorption efficiency of MgAl-LDH is improved when zinc or iron is added to the composition. A quaternary CaMgAlFe-LDH was prepared from steel making slag raw materials and utilized for methyl orange removal (Wang et al. 2016).

Furthermore, many studies reported that adsorption capacity of the LDH samples was increased after the calcination process mainly due to the increase in the surface area (Ni et al. 2007; Extremera et al. 2012; Li et al. 2016). In the study of Li et al. (2016), MgAl-LDH was used for Congo red removal and the maximum adsorption capacity was reported as 129.9 mg/g and 143.27 mg/g for pristine and calcined samples, respectively. In another study, the maximum adsorption capacity of NiMgAl-LDH for Congo red was found to be higher as 303 mg/g and 1250 mg/g for pristine and calcined samples, respectively, showing an increment in both the surface area, hence the adsorption capacity due to nickel addition (Lei et al. 2017). In another study, much higher adsorption capacity for methyl orange was obtained with calcined MgNiAl-LDH in comparison to the pristine LDH (Zaghouane-Boudiaf et al. 2012).

Aissat et al. (2018) studied the adsorption of Alizarin Red S Dye on calcined MgAl, ZnAl, and MgZnAl and reported that ZnAl achieved the highest amount of dye adsorbed followed by MgAl and then MgZnAl. In another study of Flores et al. (2011), both pristine and calcined MgAl and MgZnAl were elucidated as an adsorbent for RBBR and Direct Red; however, the study mainly focused on the kinetics. Up to date, a

comparative study on dye adsorption capacities of divalent MgAl, ZnAl, and ternary ZnMgAl in both pristine and calcined form focusing on the adsorbent characteristics and adsorption mechanisms has not yet been conducted. Moreover, a comparative investigation of the surface charge of the divalent and ternary LDH samples is required to provide a better understanding of the related adsorption mechanism.

This is the first comprehensive study investigating RBBR adsorption on pristine and calcined MgAl, ZnAl, and ZnMgAl elucidating the characteristics of the LDHs and adsorption mechanisms. RBBR is selected as a representative reactive dye not only due its reactive and toxic properties but also due to the limited studies available on the adsorption of RBBR on LDH (Flores et al. 2011; Elkhattabi et al. 2013). Pristine and calcined MgAl, ZnAl, and ZnMgAl LDHs were tested individually for the adsorption of RBBR in aqueous solution. The characteristics of all LDH samples were studied by XRD, FTIR, BET method, and zeta potential analyzer in order to elucidate the mechanisms responsible for RBBR adsorption.

2 Experimental Methodology

2.1 Materials

Analytical grade $Mg(NO_3)_2 \cdot 6H_2O$, $Zn(NO_3)_2 \cdot 4H_2O$, and $Al(NO_3)_3 \cdot 9H_2O$ were supplied from Merck (Darmstadt, Germany), while Remazol Brilliant Blue Reactive (RBBR) ($C_{22}H_{16}N_2Na_2O_{11}S_3$, 50%) was supplied from Sigma-Aldrich (USA). Standard working solutions of required concentrations were prepared by dilution with distilled water produced using Sartorius 61316 and 611 UV ultrapure water system (UK). The characteristics of the RBBR dye are presented in Table 1.

2.2 Preparation of the LDHs

Three different LDH of ZnAl, MgAl, and ZnMgAl, were prepared by coprecipitation method with a molar ratio of 3:1 as described by Theiss et al. (2016). For the synthesis of divalent ZnAl and MgAl, 100 mL of aqueous solution containing 5 M NaOH and 1 M $NaCO_3$ was added dropwise into a 100 mL solution of $Mg(NO_3)_2 \cdot 6H_2O$ or $Zn(NO_3)_2 \cdot 4H_2O$ (0.75 M) and $Al(NO_3)_3 \cdot 9H_2O$ (0.25 M), respectively. Triple-metal
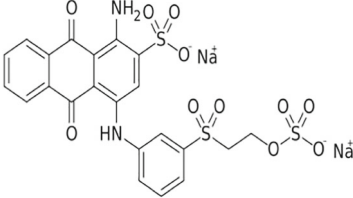
(ternary) ZnMgAl-LDH was prepared with $Mg(NO_3)_2 \cdot 6H_2O$ (0.375 M), $Zn(NO_3)_2 \cdot 4H_2O$ (0.375 M), and $Al(NO_3)_3 \cdot 9H_2O$ (0.25 M) with a ratio of 1.5:1.5:1, respectively. All the LDH samples were prepared under vigorous stirring until a final pH value of 10 ± 0.5 was attained as described by dos Santos et al. (2017). During the synthesis, the solution was purged by N_2 while the solution was being stirred for about 30 min. The slurry formed was aged at 60 °C for 24 h. Afterwards, the samples were centrifuged at 3000 rpm ($1008 \times g$) for 15 min and washed with distilled water until when the solution pH 7 was achieved for the washing solution. The LDH samples obtained were then oven dried at 80 °C for 24 h, ground and sieved with a mesh size of 100 mm. The calcined LDHs denoted as MgAl-C, ZnAl-C, and ZnMgAl-C LDHs were prepared by calcining the LDH samples in a muffle furnace at 500 °C for 4 h.

2.3 Characterization of the LDHs

X-ray diffraction pattern measurements for the LDH samples were performed with an Ultima IV powder X-ray diffractometer (XRD) (Rigaku, Japan) operating at 40 kV, 30 mA with monochromatized $CuK\alpha$ radiation ($\lambda = 0.15406$ nm), in the reflection scanning mode from $2\theta = 10°$ to $80°$ at a scan rate of $1°/min$. Fourier transform infrared (FT-IR) spectra were recorded in the wavelength range of 400–4000 cm^{-1} using an IR Prestige-21 FT-IR Spectrophotometer (Shimadzu, Japan). Both XRD and FT-IR analysis were conducted before and after the RBBR adsorption on both pristine and calcined LDH samples.

The specific surface area (S_{BET}), pore size distribution, and pore volume were analyzed using Nova Quantachrome (4000) USA, by nitrogen adsorption at 150 °C. The measurements were taken after degassing each sample at 200 °C for 5 h. S_{BET} of each sample was calculated by a multi-point BET method (Brunauer et al. 1938). Pore volume of the samples was evaluated using nitrogen adsorption and desorption method at a relative pressure (P/P_0) of 0.99, and average pore size was calculated using Barrett–Joyner–Halenda (BJH) method (Barrett et al. 1951). Zeta potential analysis of the LDH samples was performed under varied solution pH between pH 3 and pH 12 using a Zetasizer Nano-ZS (Malvern, UK), taking the mean of 3 measurements.

Table 1 Characteristics of RBBR

Name	Molecular Formula&(Molecular Weight, g/mol)	Chemical Structure	Molecular Width&Length& Height (A°)	pK_a
Remazol Brilliant Blue Reactive (RBBR)	$C_{22}H_{16}N_2Na_2O_{11}S_3$ (626.5)		13&26&8.5[a] 11.3&18.4[b]	<1[c]

[a](Yahya et al. 2016)
[b](Silva et al., 2016)
[c](Saquib and Muneer 2002; Momenzadeh et al. 2011)

[a] Yahya et al. (2016)

[b] Silva et al. (2016)

[c] Saquib and Muneer (2002); Momenzadeh et al. (2011)

2.4 Adsorption Experiments

For the batch adsorption experiments, a stock solution of 1000 mg/L RBBR was prepared. Experimental solutions of 300 mL with dye concentrations of 10, 25, 50, 75, 100, 125, 150, 175, 200, and 250 mg/L were prepared using the stock solution. After the addition of 0.5 g/L of LDH, the solutions were placed in a water bath at 25 °C and mixed at 200 rpm. The solution pH was varied between pH 3 and pH 12 for the pH experiments while it was kept constant at pH 7 for the rest of the experiments. For the pH adjustment, 1 M NaOH and 1 M HCl were used. Following the addition of LDH, 4 mL of samples were taken at various time intervals during the experiment. The samples taken were centrifuged for 10 min at 4000 rpm (1792×g) and 25 °C. The absorbance of the RBBR in the supernatant solutions was measured using a UV-2450 UV-visible spectrophotometer (Schimadzu, Japan) at the wavelength of maximum light absorption (λ_{max}) of 591 nm. The calibration curve with $R^2 > 0.99$ for RBBR was obtained for a concentration range of 5 to 50 mg/L. The solutions with dye concentrations above the calibration curve range were diluted accordingly before the analysis.

2.5 Data Analysis

The amount of RBBR adsorbed on LDH, q_t (mg/g) at a specified time (t) (min) was determined using Eq. 1, where C_o and C_t are the initial dye concentration (mg/L) and the dye concentration at a specified time, respectively, V (L) is the volume of the dye solution, and M is the mass of the LDH.

$$q_t = \frac{(C_0 - C_t)V}{M} \tag{1}$$

The mass of RBBR adsorbed at equilibrium q_e (mg/g) onto the LDH material was calculated using Eq. 2, where C_e (mg/L) is the equilibrium dye concentration.

$$q_e = \frac{(C_0 - C_e)V}{M} \tag{2}$$

For the adsorption kinetics, the nonlinear form of the pseudo first order of Lagergren (Eq. 3), second-order reaction model (Eq. 4), intraparticle diffusion (Eq. 5), and Elovich chemisorption model (Eq. 6) where k_1 (1/min) and k_2 (g/mg min) are the rate constants, C_i is the intercept related to boundary layer effect (mg/g), and K_{id} is the intraparticle diffusion rate constant (mg/g min$^{1/2}$), α (mg/g min) is the initial adsorption rate, and

β (g/mg) is related to the extent of surface coverage and the activation energy involved in chemisorption.

$$Q_t = Q_e \left(1 - e^{-k_1 t}\right) \tag{3}$$

$$Q_t = \frac{Q_e^2 k_2 t}{1 + k_2 Q_e t} \tag{4}$$

$$Qt = K_{id} t^{0.5} + Ci \tag{5}$$

$$Q_t = \frac{1}{\beta} ln(1 + \alpha\beta t) \tag{6}$$

The nonlinear form of Freundlich (Eq. 7), Langmuir (Eq. 8), Redlich–Peterson (Eq. 9), Dubinin–Radushkevich (Eq. 10), and Temkin (Eq. 11) isotherm models were used to describe the adsorption of RBBR on LDH samples, where k_F and n are the Freundlich constants indicating the dye adsorption capacity and intensity, Q_m (mg/g) is the maximum dye adsorption capacity of LDH, and k_L (L/mg) is the Langmuir constant, K_{RP} (L/g), a_{RP} (mgl/L)$^{-g}$ are the Redlich–Peterson constants, and g is the dimensionless exponent the value of which should be $0 < g \leq 1$, Q_{DR} (mg/g) is the adsorption capacity, K_{DR} (mol^2/kJ^2) is a constant related to the adsorption energy, E (kJ/mol) is the mean adsorption energy which can be obtained by $\frac{1}{\sqrt{2K_{DR}}}$, and ε is the Polanyi potential, where $\varepsilon = RTln\left(1 + \frac{1}{C_e}\right)$ and R (8.314 J/mol K) is the gas constant and T (K°) is the absolute operational temperature, A (1/g) is the binding constant at equilibrium which corresponds to the maximum binding energy, $B = RT/b$ that corresponds to enthalpy of adsorption and b (J/mol) is the constant related to the heat of adsorption.

$$Q_e = k_F C^{1/n} \tag{7}$$

$$Q_e = \frac{Q_m k_L C_e}{1 + k_L C_e} \tag{8}$$

$$Q_e = \frac{K_{RP} C_e}{1 + a_{RP} C_e^g} \tag{9}$$

$$Q_e = Q_{DR} e^{-K_{DR}\varepsilon^2} \tag{10}$$

$$Qe = Bln(ACe) \tag{11}$$

Adsorption experiments were finalized when at least two consecutive similar equilibrium dye concentrations were obtained. All experiments were run in duplicate to ensure the reproducibility of the data. The average of the two experimental results was reported together with the variability as represented with the error bars on the figures.

3 Results and Discussion

3.1 Characteristics of LDHs

The surface charge of the LDH samples was investigated by measuring the zeta potential in aqueous media at various solution pH as shown in Fig. 1. The data demonstrate that pristine and calcined ZnAl, MgAl, and ZnMgAl had a zero point charge (zpc) between solution pH 8 and pH 10. Hence, LDH samples were positively charged up to pH 8 while at solution pH above pH 10, negative surface charge dominated. At all pH values tested, zeta potential of all pristine LDH samples was similar to each other. However, for the calcined ones, ZnMgAl-C had a higher positive zeta potential compared to ZnAl-C and MgAl-C at all pH up to pH 10. Notably, all calcined samples had higher positive charge than the charge of the pristine ones at all solution pH up to pH 7. The higher positive charge of the calcined samples can be attributed to the loss of charge compensating anions during the calcination process.

The N_2 adsorption–desorption isotherms for the pristine and calcined MgAl, ZnAl, and ZnMgAl are shown in Supporting Information (Fig. S1). The isotherms of both pristine and calcined LDHs can be defined as type IV adsorption with H3 hysteresis loops according to IUPAC classification (Pourfaraj et al. 2017), indicating that all the LDH samples were formed of aggregates of plate like particles and gave rise to silt shape pores (El Hassani et al. 2017). The surface area (S$_{BET}$), pore volume (V$_{pore}$), and average pore diameter (d$_{pore}$) of pristine and calcined samples are presented in Table 2.

All three pristine samples had similar surface area around 40–50 m^2/g. Calcination resulted in an increase in surface area, pore volume and pore diameter for all
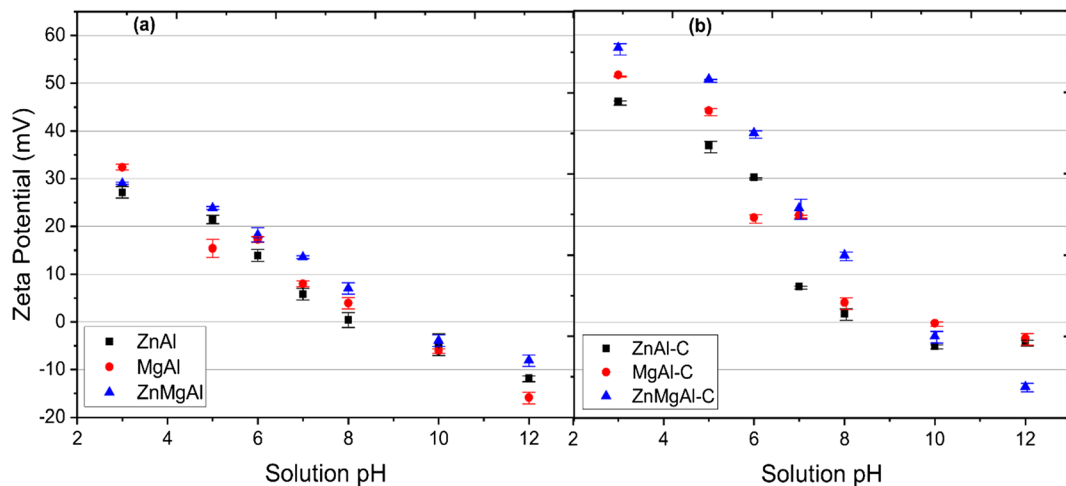
Fig. 1 Zeta potential of **a** pristine (ZnAl, MgAl, and ZnMgAl) and **b** calcined (ZnAl-C, MgAl-C, and ZnMgAl-C) LDHs versus solution pH

LDHs tested. The largest difference was observed for ZnMgAl with an increase from 50 m²/g for pristine sample to 156 m²/g for the calcined one. Similarly, a considerable increase in the surface area of various LDHs after calcination was reported by other studies (Extremera et al. 2012; Shan et al. 2015; dos Santos et al. 2017). In this study, the largest surface area was reported for ZnMgAl-C (156 m²/g), followed by MgAl-C (118 m²/g) and then ZnAl-C (109 m²/g). The data show that ZnMgAl-C had the highest pore volume of 0.54 cm³/g while ZnAl had the lowest (0.25 cm³/g). Higher surface area and hierarchical pore structure are expected to provide more active sites for anionic dyes, hence enhance the adsorption capacity (Lei et al. 2017).

FTIR spectra of pristine MgAl, ZnAl, and ZnMgAl presented in Fig. 2 show strong and intense broad adsorption bands at around 3448 cm⁻¹, 3451 cm⁻¹, and 3465 cm⁻¹ ascribed to OH⁻ groups as similarly reported in other studies (Ling et al. 2016; Iftekhar et al. 2018; Oladipo et al. 2019). The symmetry vibration band

observed at 1650 cm⁻¹ for MgAl was assigned to water molecule as reported by Meng et al. (2015) while the intense peaks around 1362 cm⁻¹, 1354 cm⁻¹, and 1356 cm⁻¹ were indications of carbonate groups for ZnAl, MgAl, and ZnMgAl, respectively, in compliance with the peaks reported by Iftekhar et al. (2018). The lower band frequencies between 500 and 1000 cm⁻¹ correspond to M-O and M-O-M stretching related to the layers of the LDH (Ling et al. 2016; Ifebajo et al. 2019). After calcination, the loss of the interlayer anions in LDH structure was observed by the disappearance of spectra peaks related to hydroxyl and carbonate groups as shown in Fig. 2.

The XRD data of pristine and calcined samples are illustrated in Fig. 3 and demonstrate that the samples have a hydrotalcite-like structure based on the diffraction pattern corresponding to the one in Joint Committee on Powder Diffraction Standards (JCPDS) as ZnAl (JCPDS 00-0358-0486), MgAl (JCPDS 00-035-0965), ZnMgAl (JCPDS 00-048-1023, JCPDS no 00-035-0821), ZnAl-C (JCPDS 00-051-0037), MgAl-C (JCPDS 01-079-0612), and ZnMgAl-C (JCPDS 03-065-4596). The major peak planes (003 and 006) in all three pristine samples at low 2θ angle correspond to the stacking order of the layers, while the peaks at higher 2θ (between 60 and 65 °C) is due to (110) plane as reported in the literature (Chagas et al. 2015; Li et al. 2016; Mahjoubi et al. 2017). The interlayer spaces (d(003)) of ZnAl, MgAl, and ZnMgAl were determined as 7.60 Å, 7.74 Å, and 7.64 Å, respectively (Table 4). Slightly lower interlayer space of Zn containing LDHs is due to the increased layer charge density as Zn is more

Table 2 Surface area, pore volume, and average pore diameter of pristine and calcined LDH samples

Samples	S_{BET} (m² g⁻¹)	V_{pore} (cm³ g⁻¹)	d_{pore} (nm)
ZnAl	44.24	0.25	22.2
MgAl	41.34	0.31	30.3
ZnMgAl	50.17	0.46	36.6
ZnAl-C	109.5	0.32	31.9
MgAl-C	117.6	0.47	32.2
ZnMgAl-C	156.2	0.54	38.6

Fig. 2 FTIR spectrum of pristine (ZnAl, MgAl, and ZnMgAl) and calcined (ZnAl-C, MgAl-C, and ZnMgAl-C) LDH samples
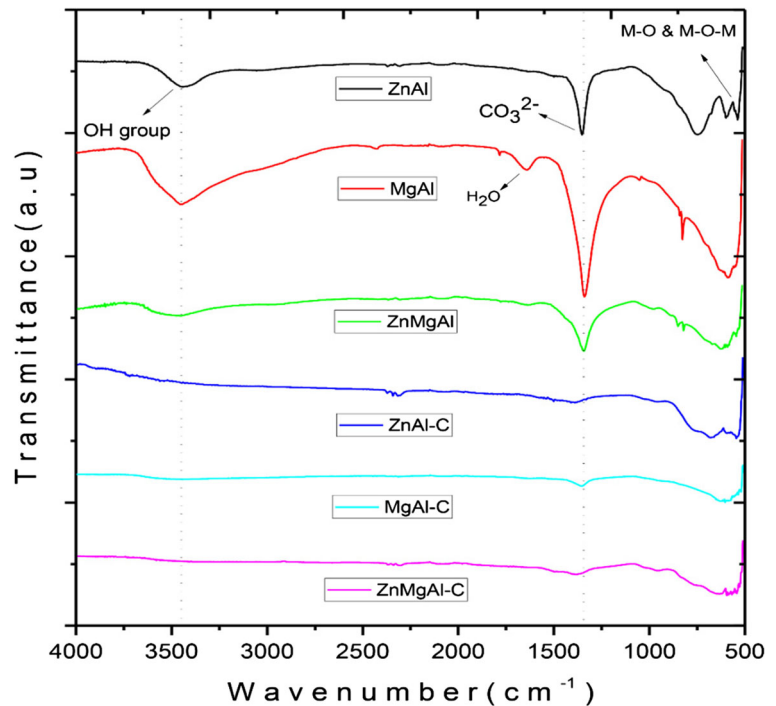
electronegative than Al (Flores et al. 2011). After calcination, transformation of the layered structure to a mixed metal oxide structure was observed. This observation was due to the disappearance of the major peaks (003 and 006), indicating that the LDH samples lost their original structure in compliance with the literature (Ni et al. 2007).
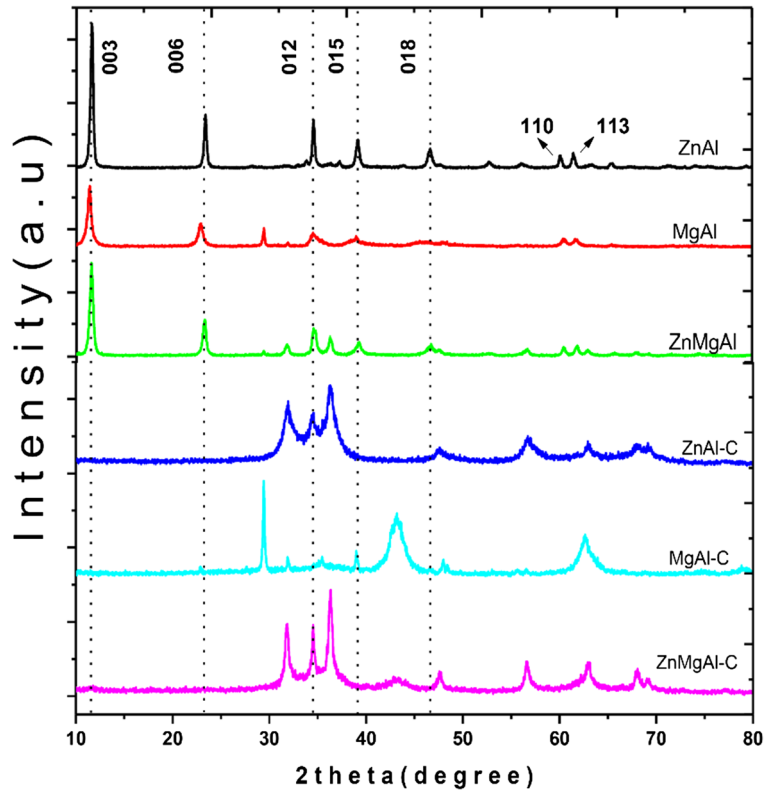
3.2 The Influence of Solution pH on RBBR Adsorption

The influence of solution pH on RBBR adsorption on pristine and calcined LDH samples at an initial dye concentration of 50 mg/L is shown in Fig. 4. The highest mass of RBBR was adsorbed at solution pH 6–8 for both pristine and calcined ZnAl and MgAl while it was at pH 7 for pristine and calcined ZnMgAl. In solutions with pH < 6 and pH > 8, the RBBR mass adsorbed declined considerably for all LDHs tested.

At solution pH 7, the adsorption capacity was 91 mg/g, 98 mg/g, and 75 mg/g for ZnAl, MgAl, and ZnMgAl and 94 mg/g, 98 mg/g, and 99 mg/g for ZnAl-C, MgAl-C, and ZnMgAl-C, respectively. Adsorption capacity of the calcined divalent LDHs (ZnAl and MgAl) did not show a considerable difference compared to the pristine ones at all studied pH values. However, a clear increase in RBBR mass

adsorbed from 75 to 99 mg/g was noted after the calcination of ZnMgAl. Similarly, in the study of Flores et al. (2011), the presence of Zn in calcined ZnMgAl improved the adsorption capacity of the LDH for dyes. In solution with a pH below 6, the decrease in the adsorption capacity for all pristine and calcined samples could be due to the dissolution of the LDH samples (Elkhattabi et al. 2013; Iftekhar et al. 2018). In addition, at lower pH values, Cl⁻ ions might be competing with the dye molecules for the sorption sites. The decline in the RBBR mass adsorbed in alkaline conditions (pH > 10) was mainly attributed to the electrostatic interactions. Up to solution pH 8, all LDHs tested had a positive zeta potential (Fig. 1) attracting the negatively charged RBBR molecules which have a low pK_a value of ~ 1 (Table 1). At solution pH above pH_{zpc}, the LDH samples became negatively charged, hence repulsing the negatively charged RBBR molecules hindering the adsorption process. The results demonstrate that electrostatic interactions are playing an important role as a mechanism for the RBBR adsorption on LDH. Besides electrostatic interactions, competition effects of OH⁻ ions could also influence the adsorption capacity of the LDHs (Berraho et al. 2016; Pourfaraj et al. 2017; Boubakri et al. 2018). Such a

Fig. 3 XRD spectrum of pristine (ZnAl, MgAl and ZnMgAl) and calcined (ZnAl-C, MgAl-C, and ZnMgAl-C) LDH samples

competition effect possibly explains why RBBR mass adsorbed declined considerably above pH 7 although the pH_{zpc} of both pristine and calcined ZnMgAl was between pH 8 and pH 10.

3.3 Adsorption Kinetics

The kinetics of RBBR adsorption on pristine and calcined ZnAl, MgAl, and ZnMgAl at various solution pH
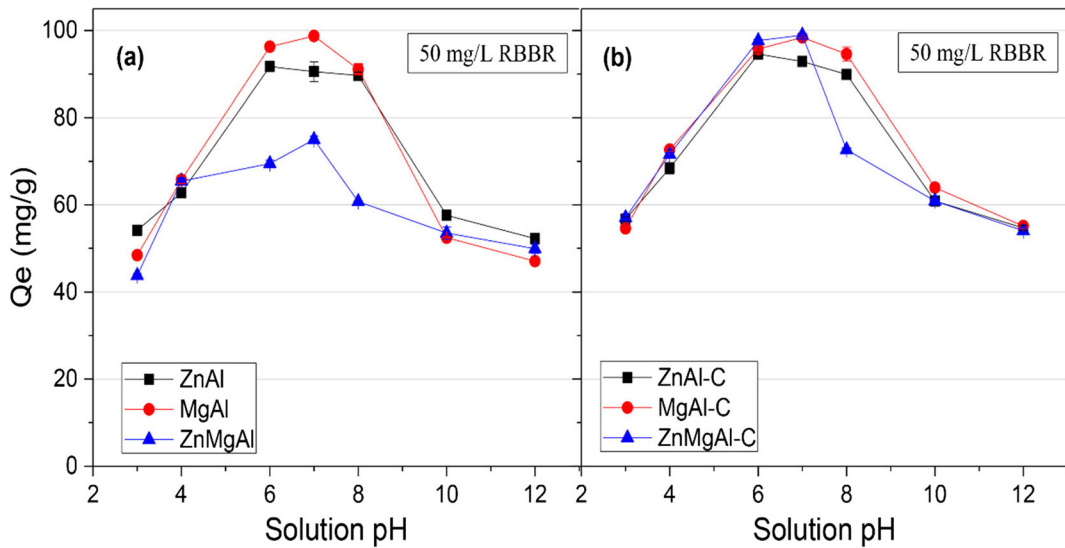

Fig. 4 The influence of solution pH on the RBBR adsorption capacity of **a** pristine (ZnAl, MgAl, and ZnMgAl) and **b** calcined (ZnAl-C, MgAl-C, and ZnMgAl-C) (50 mg/L initial RBBR concentration, sorbent load 0.5 g/L, 25 °C, 200 rpm)

and RBBR concentrations are shown in Fig. 5 and Fig. 6, respectively. At all solution pH and initial dye concentrations tested, calcined samples attained the adsorption equilibrium faster than the pristine samples.

ZnAl and MgAl reached the adsorption equilibrium in 90 min and 150 min for 10 mg/L and 250 mg/L RBBR initial concentrations, respectively. In contrast, pristine ZnMgAl sustained the equilibrium in a longer time of 120 min for 10 mg/L initial RBBR concentration while at 250 mg/L, the equilibrium time was 150 min, the same as that obtained with ZnAl and MgAl. After calcination, the equilibrium was reached in a shorter time of 40 min for 10 mg/L and 90 min for 250 mg/L, respectively, for ZnAl-C, MgAl-C, and ZnMgAl-C. When the pH experiments were considered, the ZnAl and MgAl reached the adsorption equilibrium in 120 min at solution pH 6–7. However, a longer time of 150 min was required for the equilibrium of ZnMgAl at the same pH values. For all pristine LDHs, the equilibrium was reached between 150 and 180 min for the rest of the pH values tested. However, after calcination, all three samples have sustained the equilibrium in a shorter time of 60 min at solution pH 6–7 and 120 min at other pH values studied. As observed in Fig. 1, the zeta potential of the calcined samples was higher than that of the pristine ones up to pH_{zpc}, indicating that the calcined samples were relatively more positively charged. The increased adsorption rate for the calcined samples was attributed to the enhanced electrostatic interactions because of the increased positive surface charge of the LDHs.

The equilibrium data were studied using four different kinetic models, pseudo-first order, pseudo-second order, intraparticle diffusion, and Elovich model. The adjusted coefficient of determination (R_{adj}^2) together with the model coefficients obtained are presented in Table S1 and Table S2 for various solution pH and Table S3 and Table S4 for various initial dye concentrations for pristine and calcined samples, respectively. Based on the highest R_{adj}^2 and the lowest root of mean square error (SD) values, the best fit models were decided and presented in Figs. 5 and 6. The high R_{adj}^2 (> 0.98) values obtained showed that pseudo second order and Elovich models described the adsorption kinetics better than the other models when the solution pH was varied. The experimental dye adsorption capacity $Q_{e(exp)}$, agrees well with the theoretical capacity, $Q_{e(the)}$, calculated using the second-order model equation. In addition, pseudo-second order described the kinetics

for pristine LDH samples at various initial RBBR concentrations well. However, for the calcined samples, pseudo-first order was a better model to explain the kinetics data with a R_{adj}^2 closer to unity and lower SD values. For both pH and initial dye concentration experiments, the pseudo-first and second-order rate constants, k_1 and k_2 increased an order of magnitude for the calcined samples (Table S2 and Table S4) showing that a faster adsorption rate was achieved after calcination.

3.4 Adsorption Isotherms

The RBBR adsorption isotherms on pristine and calcined LDHs are shown Fig. 7a–c for ZnAl, MgAl, and ZnMgAl, respectively. As demonstrated in Fig. 7, RBBR mass adsorbed was the same for all pristine and calcined LDHs at lower equilibrium concentrations. Nevertheless, at higher concentrations, calcined samples achieved higher amount of adsorption compared to the pristine ones. Up to 50 mg/L initial RBBR concentration; there was no difference in RBBR mass adsorbed between pristine and calcined ZnAl and MgAl. In contrast, at concentrations above 50 mg/L, calcined samples had higher adsorption capacity than the pristine samples. ZnMgAl-C obtained a higher RBBR mass adsorbed than that obtained with ZnMgAl when the initial dye concentration was above 25 mg/L.

Nonlinear form of Langmuir, Freundlich, Redlich–Peterson, Dubinin–Radushkevich, and Temkin isotherms were used to study the equilibrium data and the model coefficients are presented in Table S5. The R_{adj}^2 and adsorption isotherm constants for the best fit models are presented in Table 3. Among all the models tested, Freundlich model described the RBBR adsorption well for ZnMgAl and ZnAl-C indicating a multilayer adsorption. However, Redlich–Peterson model explained the data the best for the rest of the pristine and calcined LDHs with a higher R_{adj}^2 and a lower SD value compared to the other models. Although Redlich–Peterson model had a good fit to the equilibrium data obtained with MgAl-C with an $R_{adj}^2 > 0.97$, the model seemed to overestimate the RBBR mass adsorbed at higher equilibrium concentrations. Redlich–Peterson model is known to combine the characteristics of the Freundlich and Langmuir isotherm (Tran et al. 2017) and is postulated to fit more to Freundlich at high concentrations. RBBR possess 4 benzene rings which could contribute to hydrophobic and π-π interactions between the adsorbed molecules (Ferreira et al. 2017) promoting
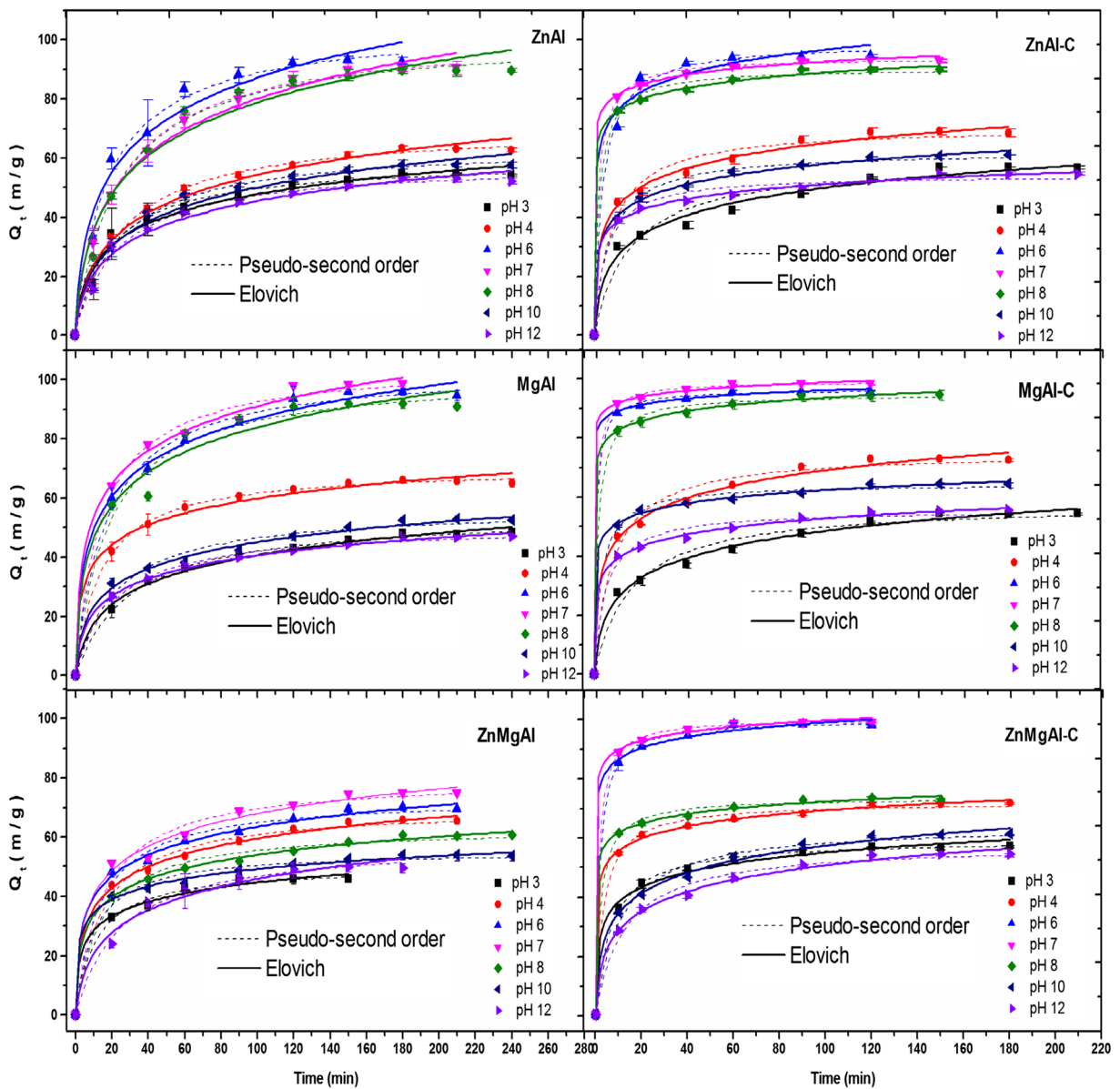
Fig. 5 Time-dependent RBBR adsorption on pristine (ZnAl, MgAl, and ZnMgAl) and calcined (ZnAl-C, MgAl-C, and ZnMgAl-C) at various solution pH with pseudo-second-order and Elovich kinetic model fits (50 mg/L initial RBBR concentration, sorbent load 0.5 g/L, 25 °C, 200 rpm)

the multilayer adsorption. However, two dye molecules are required to approach to each other in a face to face arrangement to have more chances for π-π interactions. Such an approach could be possible due to the strong electrostatic interaction between the positively charged LDH and the negatively charged RBBR molecules.

When the pristine samples were compared, the largest RBBR mass adsorbed was obtained with MgAl (220 mg/g) followed by ZnAl (191 mg/g) and ZnMgAl

(164 mg/g). The surface area and charge of the pristine samples were comparable to each other as shown in Table 2 and Fig. 1, respectively. The difference between the surface areas and charge of the samples was not large enough to cause a variation in the adsorption capacity. Yang et al. (2005) reported that the competing ions had stronger effect during adsorption on the pristine LDHs than the calcined ones. Ion competition was possibly more influential for pristine ZnMgAl
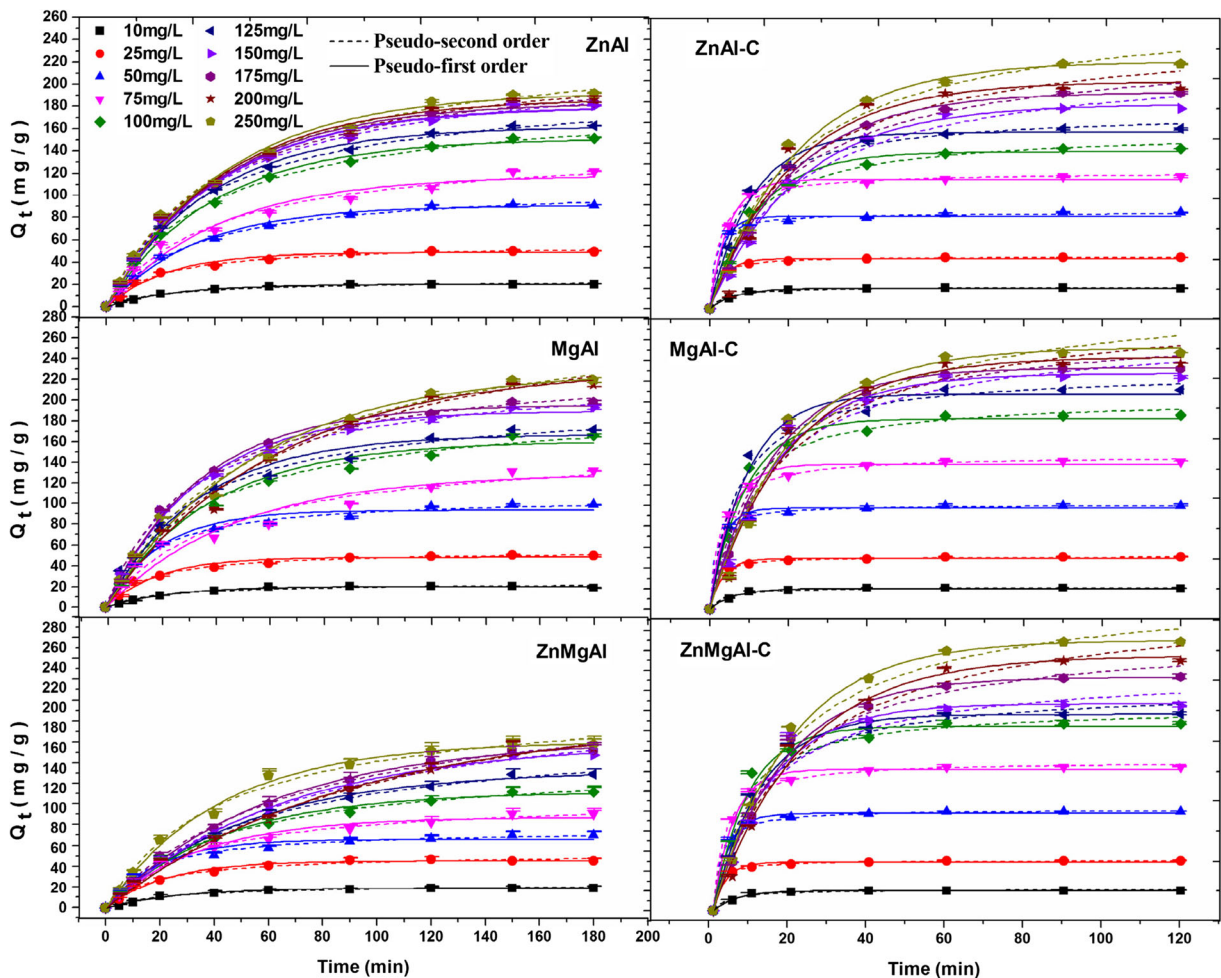
Fig. 6 Time-dependent RBBR adsorption on pristine (ZnAl, MgAl, and ZnMgAl) and calcined (ZnAl-C, MgAl-C and ZnMgAl-C) at various initial dye concentration with pseudo- first- and second-order kinetic model fit (pH 7, sorbent load 0.5 g/L, 25 °C, 200 rpm)

explaining why RBBR adsorption on ZnMgAl was hindered more in comparison to ZnAl and MgAl. After calcination, the surface area of the calcined samples increased considerably, especially for ZnMgAl-C, hence improving the adsorption capacity. Similarly, enhanced adsorption due to the increase in surface area of various LDH samples after calcination was reported in the literature (Extremera et al. 2012). ZnMgAl-C adsorbed the largest mass of RBBR (263 mg/g) followed by MgAl (247 mg/g) and then ZnAl (236 mg/g). The adsorption capacity of the calcined samples can be directly correlated to the available surface area of the samples in the order of 156 m²/g, 118 m²/g, and 109 m²/g for ZnMgAl, MgAl, and ZnAl, respectively. The superior adsorption capacity of ZnMgAl-C can be attributed to different factors. Firstly, the surface area of the ZnMgAl-C

was tripled to 156 m²/g, considerably larger than that of ZnAl-C and MgAl-C. Secondly, the increase in zeta potential after calcination was higher for ZnMgAl-C in comparison to that for ZnAl-C and MgAl-C; hence, stronger electrostatic interactions can explain the enhanced capacity of ZnMgAl-C. Lastly, Liu et al. (2012), reported that metal oxides show good selectivity to acid dyes due to their increased basicity; hence, increased basicity of the LDH after calcination is expected. Casenave et al. (2001) showed that Ni enhanced MgAl shows a synergic effect of improved basicity after calcination. Similarly, in this study, ZnMgAl-C possibly have similar properties of higher basicity adsorbing considerably larger mass of acidic RBBR in comparison to the divalent LDH samples.
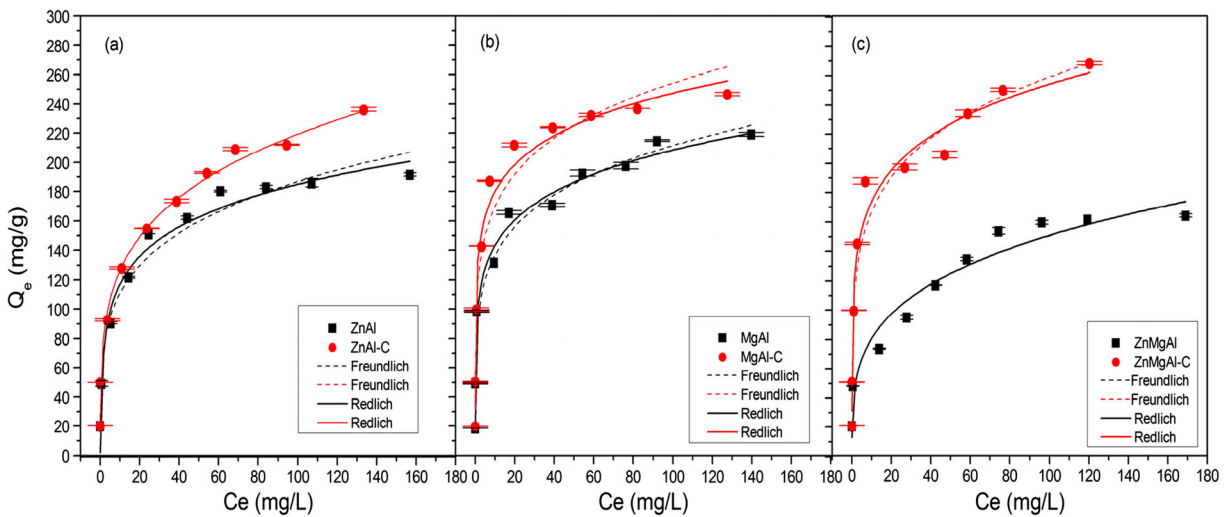
Fig. 7 Freundlich and Redlich–Peterson isotherm models for RBBR adsorption on **a** ZnAl and ZnAl-C, **b** MgAl and MgAl-C, and **c** ZnMgAl and ZnMgAl-C (pH 7, sorbent load 0.5 g/L, 25 °C, 200 rpm)

3.5 Adsorption Mechanisms

LDHs are known to adsorb anions from the aqueous solution via several adsorption mechanisms: interlayer anion exchange, memory effect, surface adsorption, electrostatic interaction, and hydrogen bonding (Goh et al. 2008; Zubair et al. 2017). Pseudo-second-order and Elovich models suggest that chemisorption is the responsible mechanism for RBBR adsorption on pristine and calcined LDHs tested (Ifebajo et al. 2019). Equilibrium studies showed that Redlich–Peterson isotherm described the data the best for most of the pristine and calcined samples except the two which were described by the Freundlich isotherm well. Redlich–Peterson isotherm is known to combine the characteristics of Langmuir and Freundlich isotherms indicating that the adsorption takes place by the combination of both physical and chemical interactions. It is well known that kinetic and isotherm model fits alone are not sufficient to conclude on the adsorption mechanisms. In this study, results of the solution pH and zeta potential studies showed that electrostatic interactions play a significant role for RBBR adsorption on all samples especially for the calcined LDHs. In order to determine the removal mechanisms further, XRD and FT-IR analysis of the samples before and after RBBR adsorption were conducted. The XRD spectra for the samples are presented in Fig. 8.

Table 3 Freundlich and Redlich–Peterson isotherm model constants and correlation coefficients for adsorption of RBBR on pristine and calcined ZnAl, MgAl, and ZnMgAl (pH 7, sorbent load 0.5 g/L, 25 °C, 200 rpm)

Models*	Parameters	Units	ZnAl	MgAl	ZnMgAl	ZnAl-C	MgAl-C	ZnMgAl-C
Freundlich	R_{adj}^2		0.971	0.977	0.955	0.991	0.948	0.954
	K_F		66.4	89.3	43.2	73.4	114.4	107.6
	n		4.434	5.324	3.682	4.194	5.742	5.240
	SD		10.52	10.59	10.91	6.95	18.93	18.15
Redlich–Peterson	R_{adj}^2		0.971	0.988	n.a.	n.a.	0.974	0.962
	K_{RP}	L/g	184.6	3912.9			3540.1	4040.4
	a_{RP}	$(mgl/L)^{-g}$	2.18	39.01			26.59	33.63
	g		0.827	0.840			0.865	0.837
	SD		10.45	7.63			13.42	15.92

R_{adj}^2 adj. R-square, SD square root of reduced chi squared, *n.a.* the model failed to fit the data
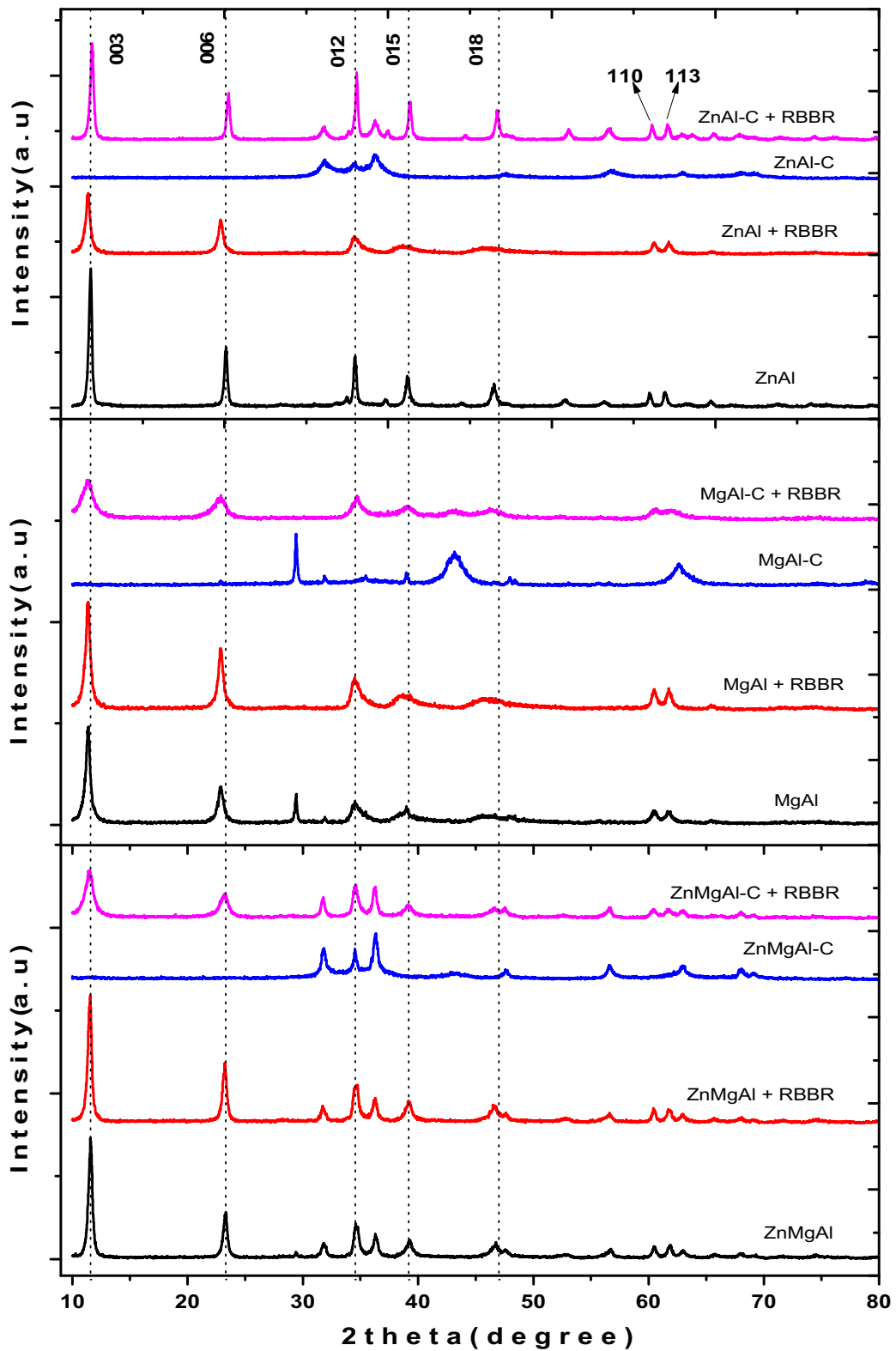
*The isotherm models were applied using Origin Pro 9.0

Fig. 8 XRD spectrum of pristine (ZnAl, MgAl, and ZnMgAl) and calcined (ZnAl-C, MgAl-C, and ZnMgAl-C) before and after RBBR adsorption

Table 4 Interlayer space and lattice parameters of LDHs before and after RBBR adsorption

Samples	Inlayer space (Å)	a (Å)	c (Å)
ZnAl	7.60	3.077	22.779
MgAl	7.74	3.063	23.226
ZnMgAl	7.62	3.061	22.866
ZnAl+RBBR	7.62	3.077	22.875
MgAl+RBBR	7.77	3.065	23.304
ZnMgAl+RBBR	7.65	3.061	22.959
ZnAl-C+RBBR	7.54	3.072	22.623
MgAl-C+RBBR	7.81	3.052	23.427
ZnMgAl-C+RBBR	7.65	3.064	23.052

Lattice cell parameters are presented in Table 4 where average cation–cation distance is represented by a = 2d (110) while c = 3d (003) is the electrostatic interaction between the layers and the interlayer species. The data in Table 4 show that there was not a considerable change in the interlayer spacing after the adsorption of RBBR on both pristine and calcined samples indicating that intercalation of RBBR did not occur.

When dye adsorption takes place on LDH the basal spacing usually increases (Tezuka et al. 2004; Choy et al. 2008; Darmograi et al. 2015) as the size of the dye molecule is larger than the size of the interlayer anion. However, in this study, the basal spacing of the LDH samples after RBBR adsorption did not change and varied between 0.75 and 0.78 nm. The layer thickness of brucite-like materials was estimated as 0.48 nm (Darmograi et al. 2015). Subtracting the layer thickness of the brucite-like layer (0.48 nm) from the basal spacing, the interlayer space was calculated as 0.30 nm. When the interlayer space was compared to the molecular dimensions of RBBR (Table 1), the space available was not large enough even for the shortest dimension of RBBR molecule (0.85 nm) to be intercalated. As a result, intercalation was not a responsible mechanism for RBBR adsorption on both pristine and calcined samples indicating that adsorption was mainly achieved by surface adsorption. As observed in Fig. 8, XRD peak (003 and 006) planes for the calcined samples were recorded after the adsorption of RBBR, and this is a common phenomenon regarded as memory effect where the carbonate and hydroxyl groups are intercalated back in the calcined LDHs to reconstruct the layered structure

of the LDH after being hydrated (Ulibarri et al. 2001; Abdelkader et al. 2011).

Figure 9 shows the FTIR spectrum of RBBR dye, pristine and calcined samples before and after the adsorption of RBBR. The spectrum of RBBR presents a peak near 1500 cm^{-1} and 1600 cm^{-1} for the C=C-C aromatic ring stretch and near 1200 cm^{-1} and 1100 cm^{-1} for S=O vibration (Elkhattabi et al. 2013). The presence of S=O vibration on both pristine and calcined samples after the adsorption indicated that RBBR molecules were adsorbed on LDH supporting chemisorption as a mechanism. The peaks for hydroxyl and carbonate groups were not present for the calcined samples before adsorption. After RBBR adsorption, the peaks for O-H groups appeared due to the hydration of the calcined samples; however, the peaks for carbonate group were missing. XRD data previously showed that intercalation of RBBR molecules did not occur and RBBR was mainly adsorbed on the surface. Adsorption possibly took place by ligand exchange where OH$^-$ or H$_2$O groups on the surface were displaced by the RBBR molecules (Lei et al. 2014). The positive charge of the LDHs was possibly balanced by the negatively charged RBBR molecules adsorbed; hence, less carbonate anions were intercalated compared to those present in the pristine samples. Similarly, for pristine samples, after adsorption, the intensity of the peaks for carbonate groups was very low in the FT-IR spectra. Reduced intensity of carbonate peaks was possibly due to the release of carbonate ions during RBBR adsorption in order to balance the charge of the LDHs as similarly reported in the literature (Casenave et al. 2001).

4 Conclusion

Pristine and calcined ZnAl, MgAl, and ZnMgAl LDH samples are tested for RBBR adsorption in aqueous media and their adsorption capacities are compared based on their characteristics. When the pristine samples are considered, ternary ZnMgAl shows the lowest performance compared to ZnAl and MgAl in terms of both RBBR mass adsorbed and adsorption rate. The surface charge and total surface area of the pristine samples are very similar to each other. Less amount of RBBR adsorbed on the ternary LDH is possibly due to the influence of
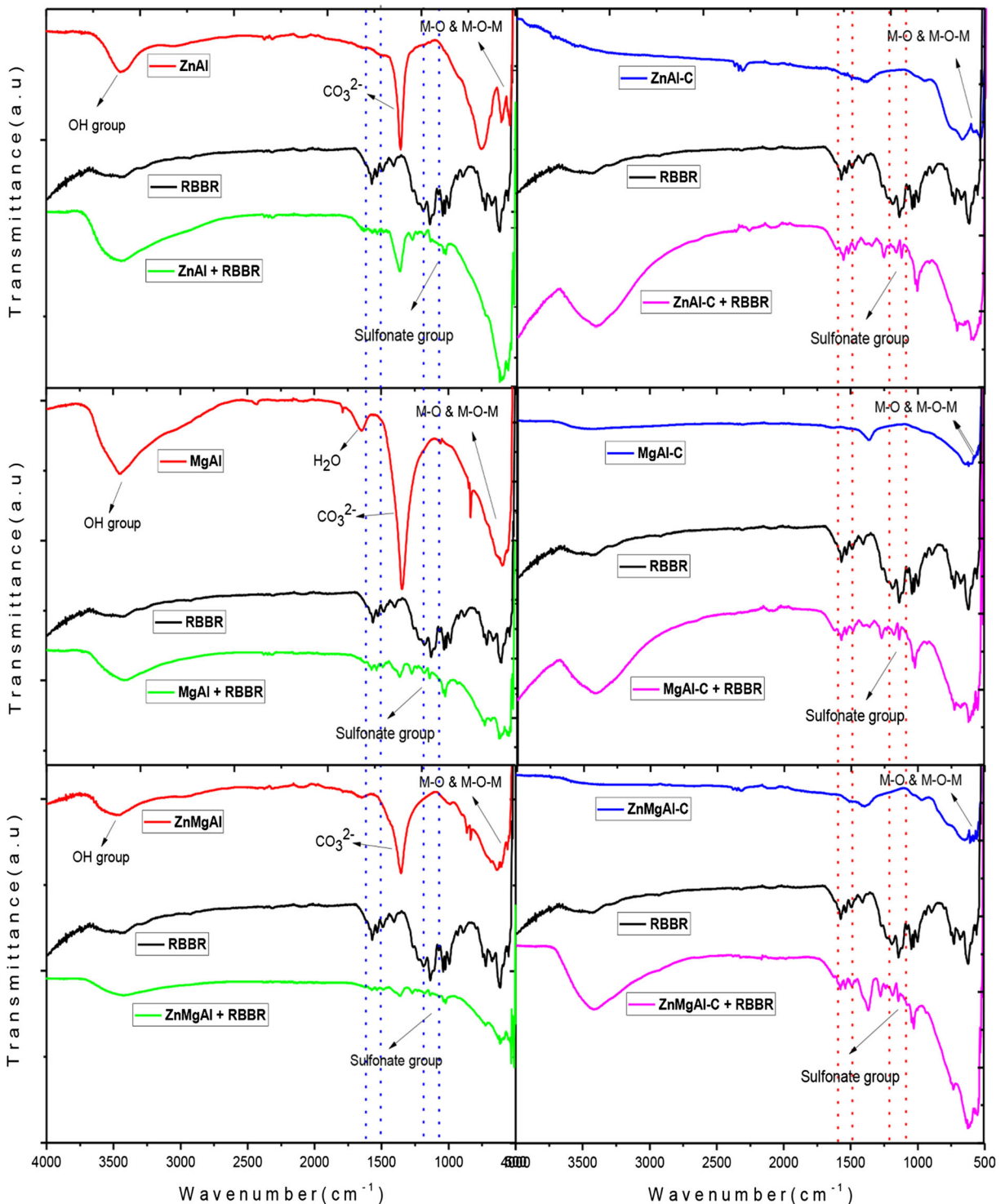
Fig. 9 FTIR spectrum of pristine (ZnAl, MgAl, and ZnMgAl) and calcined (ZnAl-C, MgAl-C, and ZnMgAl-C) before and after RBBR adsorption

the competing ions. After calcination, RBBR adsorption rate and capacity of all three LDH samples are enhanced. The increased adsorption performance of the samples is attributed to the increase in both

surface area and surface charge of all three LDHs. Nevertheless, the enhancement is superior for ZnMgAl-C compared to that of ZnAl-C and MgAl-C. This superior adsorption capacity is attributed to the fact that calcined ternary ZnMgAl-C has the highest surface area in addition to the highest positive zeta potential compared to the divalent LDHs. Intercalation of RBBR does not take place due to the molecular size of the dye molecule being larger than the interlayer space of all three LDHs tested. Conclusively, RBBR adsorption on all LDH samples in aqueous solution is achieved by surface adsorption via electrostatic interactions while intercalation does not play a role in the process.

References

Abdelkader, N. B., Bentouami, A., Derriche, Z., Bettahar, N., & Ménorval, L. D. (2011). Synthesis and characterization of Mg – Fe layer double hydroxides and its application on adsorption of Orange G from aqueous solution. *Chemical Engineering Journal, 169*(1–3), 231–238. https://doi.org/10.1016/j.cej.2011.03.019.

Abdellaoui, K., Pavlovic, I., Bouhent, M., Benhamou, A., & Barriga, C. (2017). A comparative study of the amaranth azo dye adsorption/desorption from aqueous solutions by layered double hydroxides. *Applied Clay Science, 143*, 142–150. https://doi.org/10.1016/j.clay.2017.03.019.

Aissat, M., Hamouda, S., Benhadria, N., Chellali, R., & Bettahar, N. (2018). Alizarin red S dye removal from contaminated water on calcined [Mg/Al, Zn/Al and MgZn/Al]-LDH. *AIP Conference Proceedings, 1968*(May). https://doi.org/10.1063/1.5039164.

Banat, I. M., Nigam, P., Singh, D., & Marchant, R. (1996). Microbial decolorization of textile-dye-containing effluents: A review. *Bioresource Technology, 58*(3), 217–227. https://doi.org/10.1016/S0960-8524(96)00113-7.

Barrett, E. P., Joyner, L. G., & Halenda, P. P. (1951). The determination of pore volume and area distributions in porous substances. I. Computations from Nitrogen Isotherms. *Journal of the American Chemical Society, 73*(1), 373–380. https://doi.org/10.1021/ja01145a126.

Bediako, J. K., Lin, S., Sarkar, A. K., Zhao, Y., Choi, J. W., Song, M. H., Cho, C. W., & Yun, Y. S. (2019). Evaluation of orange peel-derived activated carbons for treatment of dye-contaminated wastewater tailings. *Environmental Science*

and Pollution Research. https://doi.org/10.1007/s11356-019-07031-8.

Berraho, M., Legrouri, A., Bentaleb, K. A., El Khattabi, E., Lakraimi, M., Benaziz, L., Sabbar, E., Berraho, M., & Legrouri, A. (2016). Removal of Cr(VI) from wastewater by anionic clays. *J. Mater. Environ. Sci, 7*(8), 2886–2896 https://www.researchgate.net/publication/306168055.

Boubakri, S., Djebbi, M. A., Bouaziz, Z., Namour, P., Jaffrezic-Renault, N., Amara, A. B. H., Trabelsi-Ayadi, M., Ghorbel-Abid, I., & Kalfat, R. (2018). Removal of two anionic reactive textile dyes by adsorption into MgAl-layered double hydroxide in aqueous solutions. *Environmental Science and Pollution Research, 25*(24), 23817–23832. https://doi.org/10.1007/s11356-018-2391-6.

Brunauer, S., Emmett, P. H., & Teller, E. (1938). Adsorption of gases in multimolecular layers. *Journal of the American Chemical Society, 60*(2), 309–319. https://doi.org/10.1021/ja01269a023.

Casenave, S., Martinez, H., Guimon, C., Auroux, A., Hulea, V., Cordoneanu, A., & Dumitriu, E. (2001). Acid-base properties of Mg-Ni-Al mixed oxides using LDH as precursors. *Thermochimica Acta, 379*(1–2), 85–93. https://doi.org/10.1016/S0040-6031(01)00606-2.

Chagas, L. H., De Carvalho, G. S. G., Do Carmo, W. R., San Gil, R. A. S., Chiaro, S. S. X., Leitão, A. A., Diniz, R., De Sena, L. A., & Achete, C. A. (2015). MgCoAl and NiCoAl LDHs synthesized by the hydrothermal urea hydrolysis method: Structural characterization and thermal decomposition. *Materials Research Bulletin, 64*, 207–215. https://doi.org/10.1016/j.materresbull.2014.12.062.

Choy, J. H., Kim, Y. K., Son, Y. H., Choy, Y. B., Oh, J. M., Jung, H., & Hwang, S. J. (2008). Nanohybrids of edible dyes intercalated in ZnAl layered double hydroxides. *Journal of Physics and Chemistry of Solids, 69*(5–6), 1547–1551. https://doi.org/10.1016/j.jpcs.2007.11.009.

Darmograi, G., Prelot, B., Layrac, G., Tichit, D., Martin-Gassin, G., Salles, F., & Zajac, J. (2015). Study of adsorption and intercalation of orange-type dyes into Mg-Al layered double hydroxide. *Journal of Physical Chemistry C, 119*(41), 23388–23397. https://doi.org/10.1021/acs.jpcc.5b05510.

De Sá, F. P., Cunha, B. N., & Nunes, L. M. (2013). Effect of pH on the adsorption of Sunset Yellow FCF food dye into a layered. *Chemical Engineering Journal, 215–216*, 122–127. https://doi.org/10.1016/j.cej.2012.11.024.

dos Santos, R. M. M., Gonçalves, R. G. L., Constantino, V. R. L., Santilli, C. V., Borges, P. D., Tronto, J., & Pinto, F. G. (2017). Adsorption of Acid Yellow 42 dye on calcined layered double hydroxide: Effect of time, concentration, pH and temperature. *Applied Clay Science, 140*, 132–139.

Dudek, B., Kuśtrowski, P., Bialas, A., Natkański, P., Piwowarska, Z., Chmielarz, L., Kozak, M., & Michalik, M. (2012). Influence of textural and structural properties of Mg Al and Mg Zn Al containing hydrotalcite derived oxides on Cr(VI) adsorption capacity. *Materials Chemistry and Physics, 132*(2–3), 929–936. https://doi.org/10.1016/j.matchemphys.2011.12.037.

El Hassani, K., Beakou, B. H., Kalnina, D., Oukani, E., & Anouar, A. (2017). Effect of morphological properties of layered double hydroxides on adsorption of azo dye Methyl Orange: A comparative study. *Applied Clay Science, 140*, 124–131. https://doi.org/10.1016/j.clay.2017.02.010.

Elkhattabi, E. H., Lakraimi, M., Badreddine, M., Legrouri, A., Cherkaoui, O., & Berraho, M. (2013). Removal of Remazol blue 19 from wastewater by zinc–aluminium–chloride-layered double hydroxides. *Applied Water Science, 3*(2), 431–438. https://doi.org/10.1007/s13201-013-0092-3.

Extremera, R., Pavlovic, I., Pérez, M. R., & Barriga, C. (2012). Removal of acid orange 10 by calcined mg/Al layered double hydroxides from water and recovery of the adsorbed dye. *Chemical Engineering Journal, 213*, 392–400. https://doi.org/10.1016/j.cej.2012.10.042.

Ferreira, G. M. D., Ferreira, G. M. D., Hespanhol, M. C., de Paula Rezende, J., dos Santos Pires, A. C., Gurgel, L. V. A., & da Silva, L. H. M. (2017). Adsorption of red azo dyes on multi-walled carbon nanotubes and activated carbon: A thermodynamic study. *Colloids and Surfaces A: Physicochemical and Engineering Aspects, 529*, 531–540. https://doi.org/10.1016/j.colsurfa.2017.06.021.

Flores, J., Lima, E., Maubert, M., Aduna, E., & Rivera, J. L. (2011). Clean-up of wastes from the textile industry using anionic clays. *Clays and Clay Minerals, 59*(3), 240–249. https://doi.org/10.1346/CCMN.2011.0590303.

Forgacs, E., Cserháti, T., & Oros, G. (2004). Removal of synthetic dyes from wastewaters: A review. *Environment International, 30*(7), 953–971. https://doi.org/10.1016/j.envint.2004.02.001.

Geethakarthi, A., & Phanikumar, B. R. (2011). Industrial sludge based adsorbents / industrial byproducts in the removal of reactive dyes – A review. *International Journal of Water Resources and Environmental Engineering, 3*(January), 1–9.

Goh, K. H., Lim, T. T., & Dong, Z. (2008). Application of layered double hydroxides for removal of oxyanions: A review. *Water Research, 42*(6–7), 1343–1368. https://doi.org/10.1016/j.watres.2007.10.043.

Guo, Y., Zhu, Z., Qiu, Y., & Zhao, J. (2013). Enhanced adsorption of acid brown 14 dye on calcined Mg/Fe layered double hydroxide with memory effect. *Chemical Engineering Journal, 219*, 69–77. https://doi.org/10.1016/j.cej.2012.12.084.

Ifebajo, A. O., Oladipo, A. A., & Gazi, M. (2019). Efficient removal of tetracycline by CoO/CuFe$_2$O$_4$ derived from layered double hydroxides. *Environmental Chemistry Letters, 17*(1), 487–494. https://doi.org/10.1007/s10311-018-0781-0.

Ifebajo, A. O., Oladipo, A. A., & Gazi, M. (2020). Sun-light driven enhanced azo dye decontamination from aqueous solution by CoO − CuFe$_2$O$_4$ derived from layered double hydroxide. *Desalination and Water Treatment, 1*, 1–8. https://doi.org/10.5004/dwt.2020.25247.

Iftekhar, S., Küçük, M. E., Srivastava, V., Repo, E., & Sillanpää, M. (2018). Application of zinc-aluminium layered double hydroxides for adsorptive removal of phosphate and sulfate: Equilibrium, kinetic and thermodynamic. *Chemosphere, 209*, 470–479. https://doi.org/10.1016/j.chemosphere.2018.06.115.

Kowalik, P., Konkol, M., Kondracka, M., Próchniak, W., Bicki, R., & Wiercioch, P. (2013). Memory effect of the CuZnAl-LDH derived catalyst precursor - In situ XRD studies. *Applied Catalysis A: General, 464–465*, 339–347. https://doi.org/10.1016/j.apcata.2013.05.048.

Lei, X., Jin, M., & Williams, G. R. (2014). Layered double hydroxides in the remediation and prevention of water pollution. *Energy and Environment Focus, 3*, 4–22. https://doi.org/10.1166/eef.2014.1086.

Lei, C., Zhu, X., Zhu, B., Jiang, C., Le, Y., & Yu, J. (2017). Superb adsorption capacity of hierarchical calcined Ni/mg/Al layered double hydroxides for Congo red and Cr(VI) ions. *Journal of Hazardous Materials, 321*, 801–811. https://doi.org/10.1016/j.jhazmat.2016.09.070.

Li, B., Zhang, Y., Zhou, X., Liu, Z., Liu, Q., & Li, X. (2016). Different dye removal mechanisms between monodispersed and uniform hexagonal thin plate-like MgAl-CO32–LDH and its calcined product in efficient removal of Congo red from water. *Journal of Alloys and Compounds, 673*, 265–271. https://doi.org/10.1016/j.jallcom.2016.02.248.

Ling, F., Fang, L., Lu, Y., Gao, J., Wu, F., Zhou, M., & Hu, B. (2016). A novel CoFe layered double hydroxides adsorbent: High adsorption amount for methyl orange dye and fast removal of Cr(VI). *Microporous and Mesoporous Materials, 234*, 230–238. https://doi.org/10.1016/j.micromeso.2016.07.015.

Liu, Y., Shi, J., Peng, Q., & Li, Y. (2012). Self-assembly of ZnO nanocrystals into nanoporous pyramids: High selective adsorption and photocatalytic activity. *Journal of Materials Chemistry, 22*(14), 6539–6541. https://doi.org/10.1039/c2jm16729h.

Liu, Y., Wang, G., Yang, W., Yang, J., & Li, J. (2019). Biotemplated synthesis of hierarchically porous ZnAl-CLDH/FeWO4 for effective removal of dyes from water. *Water, Air, and Soil Pollution, 230*(4). https://doi.org/10.1007/s11270-019-4134-9.

Mahjoubi, F. Z., Khalidi, A., Abdennouri, M., & Barka, N. (2017). Zn–Al layered double hydroxides intercalated with carbonate, nitrate, chloride and sulphate ions: Synthesis, characterisation and dye removal properties. *Journal of Taibah University for Science, 11*(1), 90–100. https://doi.org/10.1016/j.jtusci.2015.10.007.

Malik, A., & Grohmann, E. (2012). Environmental protection strategies for sustainable development. *In Environmental Protection Strategies for Sustainable Development.* https://doi.org/10.1007/978-94-007-1591-2.

Meng, Z., Li, X., Lv, F., Zhang, Q., Chu, P. K., & Zhang, Y. (2015). Structure, molecular simulation, and release of aspirin from intercalated Zn-Al-layered double hydroxides. *Colloids and Surfaces B: Biointerfaces, 135*, 339–345. https://doi.org/10.1016/j.colsurfb.2015.07.069.

Ni, Z. M., Xia, S. J., Wang, L. G., Xing, F. F., & Pan, G. X. (2007). Treatment of methyl orange by calcined layered double hydroxides in aqueous solution: Adsorption property and kinetic studies. *Journal of Colloid and Interface Science, 316*(2), 284–291. https://doi.org/10.1016/j.jcis.2007.07.045.

Oladipo, A. A., Ifebajo, A. O., & Gazi, M. (2019). Magnetic LDH-based CoO–NiFe2O4 catalyst with enhanced performance and recyclability for efficient decolorization of azo dye via Fenton-like reactions. *Applied Catalysis B: Environmental, 243*, 243–252. https://doi.org/10.1016/j.apcatb.2018.10.050.

Paneysar, J. S., Sawant, S., Ip, M. H., Bhullar, S. K., Barton, S., Ambre, P., & Coutinho, E. (2019). Nanofibers for textile waste water management. *Water Practice and Technology, 14*(2), 297–310. https://doi.org/10.2166/wpt.2019.014.

Pourfaraj, R., Fatemi, S. J., Kazemi, S. Y., & Biparva, P. (2017). Synthesis of hexagonal mesoporous MgAl LDH nanoplatelets adsorbent for the effective adsorption of

Brilliant Yellow. *Journal of Colloid and Interface Science, 508*, 65–74. https://doi.org/10.1016/j.jcis.2017.07.101.

Praveen, S., GR, C., & Thomas, E. (2009). Mutagenicity testing of some commonly used azo dyes. *Applied Environmental Microbiology, 42*(4), 641–648.

Rezaee, A., Ghaneian, M. T., Khavanin, A., Hashemian, S. J., Moussavi, G. H., Ghanizadeh, G. H., & Hajizadeh, E. (2008). Photochemical oxidation of reactive blue 19 dye (RB19) in textile wastewater by UV/K2S2O8 process. *Iranian Journal of Environmental Health Science and Engineering, 5*(2), 95–100.

Sajid, M., & Basheer, C. (2016). Layered double hydroxides: Emerging sorbent materials for analytical extractions. *TrAC - Trends in Analytical Chemistry, 75*, 174–182. https://doi.org/10.1016/j.trac.2015.06.010.

Shan, R. R., Yan, L. G., Yang, Y. M., Yang, K., Yu, S. J., Yu, H. Q., Zhu, B. C., & Du, B. (2015). Highly efficient removal of three red dyes by adsorption onto Mg-Al-layered double hydroxide. *Journal of Industrial and Engineering Chemistry, 21*, 561–568. https://doi.org/10.1016/j.jiec.2014.03.019.

Sheng, T., Zhang, Z., Hu, Y., Tao, Y., Zhang, J., Shen, Z., Feng, J., & Zhang, A. (2019). Adsorption of phosphorus by using magnetic Mg–Al-, Zn–Al- and Mg–Fe-layered double hydroxides: Comparison studies and adsorption mechanism. *Environmental Science and Pollution Research, 26*(7), 7102–7114. https://doi.org/10.1007/s11356-019-04191-5.

Tezuka, S., Chitrakar, R., Sakane, K., Sonoda, A., Ooi, K., & Tomida, T. (2004). The synthesis and phosphate adsorptive properties of Mg(II)-Mn(III) layered double hydroxides and their heat-treated materials. *Bulletin of the Chemical Society of Japan, 77*(11), 2101–2107. https://doi.org/10.1246/bcsj.77.2101.

Theiss, F. L., Ayoko, G. A., & Frost, R. L. (2016). Synthesis of layered double hydroxides containing Mg^{2+}, Zn^{2+}, Ca^{2+} and Al^{3+} layer cations by co-precipitation methods - A review. *Applied Surface Science, 383*, 200–213. https://doi.org/10.1016/j.apsusc.2016.04.150.

Tran, H. N., You, S. J., Hosseini-Bandegharaei, A., & Chao, H. P. (2017). Mistakes and inconsistencies regarding adsorption of contaminants from aqueous solutions: A critical review. *Water Research, 120*, 88–116. https://doi.org/10.1016/j.watres.2017.04.014.

Ulibarri, M. A., Pavlovic, I., Barriga, C., Hermosín, M. C., & Cornejo, J. (2001). Adsorption of anionic species on hydrotalcite-like compounds: Effect of interlayer anion and crystallinity. *Applied Clay Science, 18*(1–2), 17–27. https://doi.org/10.1016/S0169-1317(00)00026-0.

Wang, C., Chen, Y., Shang, X., Hou, X., Li, H., & Guo, Z. (2016). Facile synthesis of Ca/Mg/Al/Fe layered double hydroxides using steelmaking slag as raw material. *Materials Letters, 173*, 115–118. https://doi.org/10.1016/j.matlet.2016.03.022.

Wong, Y., & Yu, J. (1999). Laccase-catalyzed decolorization of synthetic dyes. *Water Research, 33*(16), 3512–3520. https://doi.org/10.1016/S0043-1354(99)00066-4.

Yagub, M. T., Sen, T. K., Afroze, S., & Ang, H. M. (2014). Dye and its removal from aqueous solution by adsorption: A review. *Advances in Colloid and Interface Science, 209*, 172–184. https://doi.org/10.1016/j.cis.2014.04.002.

Yang, L., Shahrivari, Z., Liu, P. K. T., Sahimi, M., & Tsotsis, T. T. (2005). Removal of trace levels of arsenic and selenium from aqueous solutions by calcined and uncalcined layered double hydroxides (LDH). *Industrial and Engineering Chemistry Research, 44*(17), 6804–6815. https://doi.org/10.1021/ie049060u.

Zaghouane-Boudiaf, H., Boutahala, M., & Arab, L. (2012). Removal of methyl orange from aqueous solution by uncalcined and calcined MgNiAl layered double hydroxides (LDHs). *Chemical Engineering Journal, 187*, 142–149. https://doi.org/10.1016/j.cej.2012.01.112.

Zheng, Y. M., Li, N., & Zhang, W. D. (2012). Preparation of nanostructured microspheres of Zn-Mg-Al layered double hydroxides with high adsorption property. *Colloids and Surfaces A: Physicochemical and Engineering Aspects, 415*, 195–201. https://doi.org/10.1016/j.colsurfa.2012.10.014.

Zhou, H., Jiang, Z., Wei, S., & Liang, J. (2018). Adsorption of Cd(II) from aqueous solutions by a novel layered double hydroxide FeMnMg-LDH. *Water, Air, and Soil Pollution, 229*(3). https://doi.org/10.1007/s11270-017-3597-9.

Zhu, J., Zhu, Z., Zhang, H., Lu, H., & Qiu, Y. (2019). Calcined CoAl-layered double hydroxide as a heterogeneous catalyst for the degradation of acetaminophen and rhodamine B: Activity, stability, and mechanism. *Environmental Science and Pollution Research.* https://doi.org/10.1007/s11356-019-06390-6.

Zubair, M., Daud, M., McKay, G., Shehzad, F., & Al-Harthi, M. A. (2017). Recent progress in layered double hydroxides (LDH)-containing hybrids as adsorbents for water remediation. *Applied Clay Science, 143*(March), 279–292. https://doi.org/10.1016/j.clay.2017.04.002.